



Multiple stellar populations in Magellanic Cloud clusters – V. The split main sequence of the young cluster NGC 1866

A. P. Milone,¹ A. F. Marino,¹ F. D'Antona,² L. R. Bedin,³ G. Piotto,^{3,4} H. Jerjen,¹ J. Anderson,⁵ A. Dotter,⁶ M. Di Criscienzo² and E. P. Lagioia^{7,8}

¹Research School of Astronomy and Astrophysics, Australian National University, Canberra, ACT 2611, Australia

²Istituto Nazionale di Astrofisica – Osservatorio Astronomico di Roma, Via Frascati 33, I-00040 Monteporzio Catone, Roma, Italy

³Istituto Nazionale di Astrofisica – Osservatorio Astronomico di Padova, Vicolo dell'Osservatorio 5, Padova I-35122, Italy

⁴Dipartimento di Fisica e Astronomia 'Galileo Galilei', Univ. di Padova, Vicolo dell'Osservatorio 3, Padova I-35122, Italy

⁵Space Telescope Science Institute, 3800 San Martin Drive, Baltimore, MD 21218, USA

⁶Department of Astronomy, Harvard University, Cambridge, MA 02138, USA

⁷Instituto de Astrofísica de Canarias, E-38200 La Laguna, Tenerife, Canary Islands, Spain

⁸Department of Astrophysics, University of La Laguna, E-38200 La Laguna, Tenerife, Canary Islands, Spain

Accepted 2016 November 12. Received 2016 November 12; in original form 2016 August 18

ABSTRACT

One of the most unexpected results in the field of stellar populations of the last few years is the discovery that some Magellanic Cloud globular clusters younger than ~ 400 Myr exhibit bimodal main sequences (MSs) in their colour–magnitude diagrams (CMDs). Moreover, these young clusters host an extended main-sequence turn-off (eMSTO) in close analogy with what is observed in most $\sim 1\text{--}2$ Gyr old clusters of both Magellanic Clouds. We use high-precision *Hubble Space Telescope* photometry to study the young star cluster NGC 1866 in the Large Magellanic Cloud. We discover an eMSTO and a split MS. The analysis of the CMD reveals that (i) the blue MS is the less populous one, hosting about one-third of the total number of MS stars; (ii) red MS stars are more centrally concentrated than blue MS stars; (iii) the fraction of blue MS stars with respect to the total number of MS stars drops by a factor of ~ 2 in the upper MS with $m_{F814W} \lesssim 19.7$. The comparison between the observed CMDs and stellar models reveals that the observations are consistent with ~ 200 Myr old highly rotating stars on the red MS, with rotation close to critical value, plus a non-rotating stellar population spanning an age interval between ~ 140 and 220 Myr, on the blue MS. Noticeable, neither stellar populations with different ages only, nor coeval stellar models with different rotation rates, properly reproduce the observed split MS and eMSTO. We discuss these results in the context of the eMSTO and multiple MS phenomenon.

Key words: techniques: photometric – binaries: visual – stars: rotation – globular clusters: individual: NGC 1755, NGC 1844, NGC 1856, NGC 1866 – Magellanic Clouds.

1 INTRODUCTION

Nearly all the old globular clusters (GCs) host multiple stellar populations with typical photometric and spectroscopic features (Gratton, Sneden & Carretta 2004; Marino et al. 2015; Piotto et al. 2015; Milone et al. 2016a, and references therein). The formation of the multiple stellar populations in the early Universe is one of the main open issues of stellar astrophysics and could play an important role in the assembly of the Galaxy (e.g. Gratton, Carretta & Bragaglia 2012; Renzini et al. 2015).

In this context, the discovery that most intermediate-age star clusters in the Large and Small Magellanic Clouds (LMC, SMC) exhibit a multimodal or extended main-sequence turn-off (eMSTO; Bertelli et al. 2003; Mackey & Broby Nielsen 2007; Glatt et al. 2009; Milone et al. 2009), and in some cases dual red clumps (Girardi, Rubele & Kerber 2009) have been one of the most intriguing discoveries of the last decade in the field of stellar populations. Indeed it has been suggested that clusters with eMSTOs are the younger counterparts of the old GCs with multiple populations (e.g. Mackey et al. 2008; Keller, Mackey & Da Costa 2011).

* E-mail: milone@mso.anu.edu.au

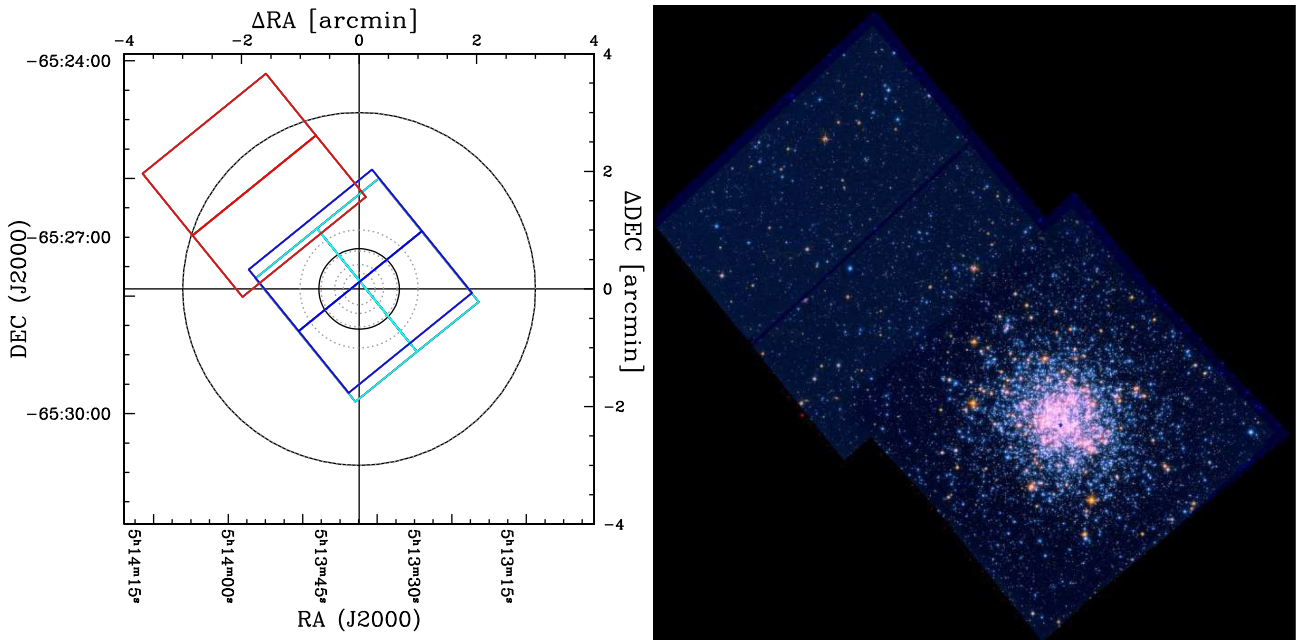


Figure 1. Left-hand panel: footprints of the UVIS/WFC3 images used in this paper. Blue, cyan, and red colours refer to images collected during different visits. The inner solid circle has a radius of 41 arcsec, corresponding to the projected cluster half-light radius, and delimits the cluster field. Reference-field stars are located outside the outer solid circle. The five dotted circles indicate the regions used to study the radial distribution of stellar populations in NGC 1866. Right-hand panel: trichromatic image of the analysed field of view.

The origin of the eMSTO has been widely investigated but a solution is still missing. A possible interpretation is that the eMSTO is due to multiple stellar populations with difference in age of about 100–700 Myr (e.g. Goudfrooij et al. 2011, 2014; Li, de Grijs & Deng 2014) and that the intermediate-age clusters have experienced a prolonged star formation episode in close analogy with old GCs (Conroy & Spergel 2011). As an alternative, the eMSTO is due to coeval multiple populations with different rotation rates (Bastian & De Mink 2009; D’Antona et al. 2015) or due to interacting binaries (Yang et al. 2011, 2013).

Recent papers, based on *Hubble Space Telescope* (*HST*) photometry, have shown that the ∼300-Myr-old cluster NGC 1856 and the ∼100-Myr-old clusters NGC 1844 and NGC 1755 exhibit a very complex colour–magnitude diagram (CMD) including split main sequence (MS) and eMSTO (Milone et al. 2013, 2015, 2016b; Correnti et al. 2015). These findings have made a clear case that the once-thought simple Magellanic Cloud (MC) young clusters host multiple stellar populations and that the eMSTO is not a peculiarity of the ∼1–2 Gyr star clusters.

The presence of multiple populations in young clusters has opened a new window of opportunity to investigate the eMSTO and has provided additional constraints to discriminate among the different scenarios. In this paper, we investigate multiple stellar populations in the ∼200 Myr old cluster NGC 1866 by using *HST* images. The paper is organized as follows. Section 2 describes the data set and the data analysis. In Sections 3 and 4, we present the CMD of NGC 1866 and investigate the cluster’s double MS, while in Section 5, we compare the observed CMD with theoretical models. A summary and discussion follow in Section 6.

2 DATA AND DATA ANALYSIS

The data set that we have used to investigate multiple stellar populations in NGC 1866 has been collected through the Ultraviolet and Visual Channel of the Wide Field Camera 3 (UVIS/WFC3) of *HST*. The footprints of these images are shown in the left-hand panel of Fig. 1 where the different colours indicate images taken during three distinct visits on 2016 March 1 (blue), 2016 May 31 (red), and 2016 June 1 (cyan). Each visit includes 2×711 s images collected through the *F336W* filter and 90 s+678 s images collected through the *F814W* filter. The inner and outer black continuous circles shown in the left-hand panel of Fig. 1 have radius of 41 (equivalent to the projected half-light radius of NGC 1866, McLaughlin & van der Marel 2005) and 180 arcsec, respectively. The region within the inner circle is mainly populated by cluster members and will be designed as cluster field hereafter. In contrast, the region outside the outer circle mostly contains field stars and is called reference field. To determine the radius of the outer circle, we have calculated the number of stars with $m_{F814W} < 22.5$ per unit area in distinct concentric annuli from the cluster centre to the outermost region of the analysed field of view. We have verified that the stellar density is constant for radial distance larger than ∼3 arcmin. This fact indicates that the number of cluster stars in the reference field is negligible. The trichromatic image of the analysed field is shown in Fig. 1.

The entire data set is part of GO-14204 (PI A. P. Milone), which is a program specifically devoted to the study of multiple stellar populations in the young LMC clusters NGC 1866 and NGC 1755 (see Milone et al. 2016b). All the images have been reduced and analysed by using the method and software programs that have been mostly developed by Jay Anderson and are widely described in previous papers from this series.

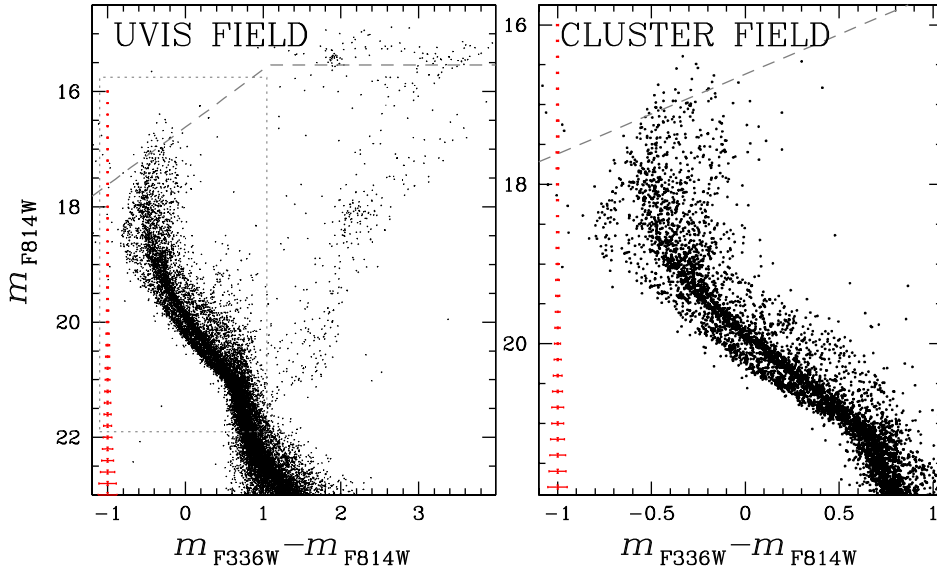


Figure 2. Left-hand panel: m_{F814W} versus $m_{F336W} - m_{F814W}$ CMD for all the stars in the WFC3/UVIS field of view. The photometry of stars above the dashed line has been obtained from saturated images in at least one filter. Right-hand panel: zoom in around the upper MS for stars with radial distance smaller than 41 arcsec from the centre of NGC 1866. The corresponding region of the CMD is marked by a dashed box in the left-hand panel plot. The error bars in red are shown on the left of each panel.

Briefly, we have first corrected the images for the effect of poor charge transfer efficiency as in Anderson & Bedin (2010) and then we have derived the stellar photometry and astrometry by using the software described in detail by Anderson et al. (2008) and adapted to UVIS/WFC3 images. Specifically, we have measured bright and faint stars by using a set of spatially variable empirical point spread functions (PSFs, see Anderson et al. 2006 for details) but by adopting two different approaches. Fluxes of bright stars have been measured in each image independently, and the results combined later, while all the pixels of each very faint star in all the images have been fitted simultaneously. Stellar positions have been corrected for geometrical distortion by using the solution provided by Bellini, Anderson & Bedin (2011) and photometry has been calibrated into the Vega-mag systems as in Bedin et al. (2005) and by adopting the zero-points provided by the STScI web page for WFC3/UVIS.¹

The sample of stars used in our study of NGC 1866 has been selected following Milone et al. (2009) and includes only relatively isolated sources that have been properly fitted by the PSF, and have small rms errors in position. Finally, the photometry of stars with radial distances smaller than 3 arcmin from the cluster centre have been corrected for differential reddening by following the recipe in Milone et al. (2012a) and adopting the values of A_{F336W} and A_{F814W} derived in Milone et al. (2016b).

In addition, we have used artificial stars (ASs) to determine the completeness level of our sample, to estimate internal photometric errors, and to derive synthetic CMD. The AS tests have been performed following the procedure of Anderson et al. (2008), while the completeness has been determined as a function of both stellar position and magnitude by following the recipes of Milone et al. (2009).

3 THE COLOUR-MAGNITUDE DIAGRAM OF NGC 1866

The m_{F814W} versus $m_{F336W} - m_{F814W}$ CMD of all the stars in the WFC3/UVIS field of view is plotted in the left-hand panel of Fig. 2, while in the right-hand panel we show a zoom around the upper part of the MS of stars in the cluster field. A visual inspection of these CMDs immediately reveals that the MSTO is broadened in colour and magnitude in close analogy with what has been observed in NGC 1856 and in the majority of the intermediate-age MC clusters (e.g. Mackey et al. 2008; Milone et al. 2009; Goudfrooij et al. 2014). Furthermore, the upper MS is clearly split, and the two MSs merge together around $m_{F814W} = 21.0$. Noticeably, the red MS hosts the majority of MS stars, similar to what we have observed in NGC 1844, NGC 1856, and NGC 1755.

In the following, we demonstrate that the split MS and the eMSTO are intrinsic features of NGC 1866. We started by comparing the Hess diagrams of stars in the cluster field and in the reference field. These diagrams are plotted in the panels (a) and (b) of Fig. 3, respectively. The adopted level of grey used in this figure is proportional to the number of stars, corrected for completeness and normalized to an area of 1 arcsec², in each interval of colour and magnitude. The panel (c) of Fig. 3 shows the Hess diagram obtained by subtracting the star counts of the panel-(b) diagram from those of the panel-(a) one. The fact that both the eMSTO and the split MS are present in the subtracted Hess diagram demonstrates that these features are real.

To further investigate the effect of field-star contamination on the cluster CMD, we have compared the panels (a) and (b) of Fig. 4 to the CMDs of stars in the cluster field and in the reference field. In order to statistically subtract the stars of the reference-field CMD from

¹ http://www.stsci.edu/hst/wfc3/phot_zp_lbn

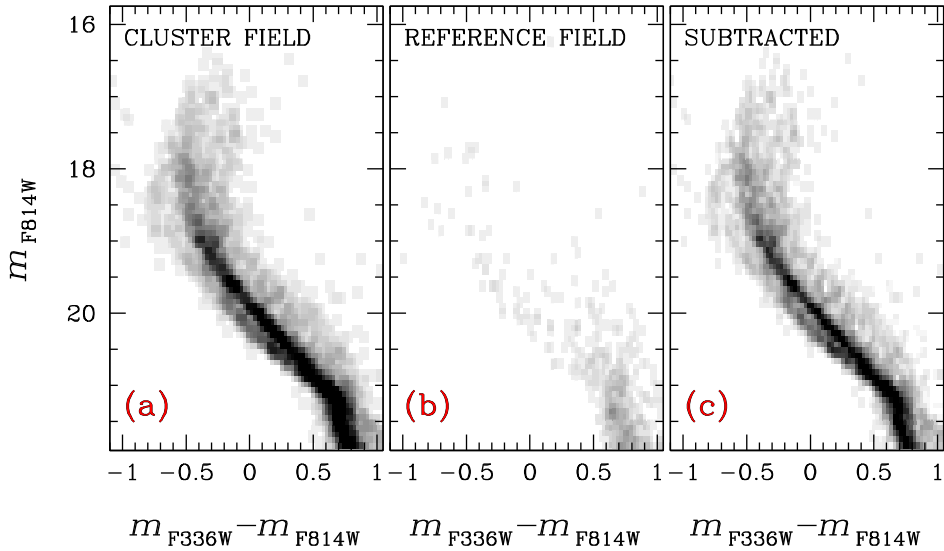


Figure 3. m_{F814W} versus $m_{F336W} - m_{F814W}$ Hess diagram of stars in the cluster field (panel a) and in the reference field (panel b). The Hess diagram of the cluster CMD after field stars have been subtracted is plotted in panel c.

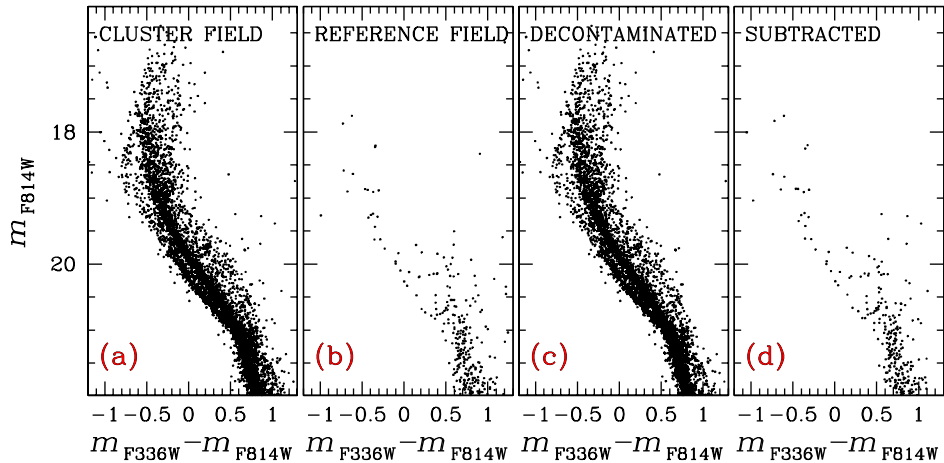


Figure 4. Panel (a) reproduces the m_{F814W} versus $m_{F336W} - m_{F814W}$ CMD of stars in the cluster field shown in the right-hand panel of Fig. 2. The CMD of stars in the reference field is plotted in panel (b), while panel (c) shows the decontaminated CMD obtained by statistically subtracting the stars of the reference field from the cluster-field CMD. The CMD of the subtracted stars is plotted in panel (d).

the cluster-field CMD, we have adapted to NGC 1866 the same procedure used by Milone et al. (2009, 2015, 2016b). Specifically, we have determined for each star (i) in the reference field a distance in the m_{F814W} versus $m_{F336W} - m_{F814W}$ CMD

$$d_i = \sqrt{k((m_{F336W,cf} - m_{F814W,cf}) - (m_{F336W,rf}^i - m_{F814W,rf}^i))^2 + (m_{F814W,cf} - m_{F814W,rf}^i)^2}$$

where $m_{F336W(F814W),cf}$ and $m_{F336W(F814W),rf}$ are the $F336W(F814W)$ magnitudes in the cluster field and in the reference field, respectively. The adopted constant $k = 4.1$ accounts for the fact that the colour of a star is better constrained than its magnitude (Gallart et al. 2003) and has been determined as in Marino et al. (2014, see their section 3.1). The stars in the cluster-field CMD with the smallest distance to each star of the reference field have been considered as candidate to be subtracted. We have subtracted all the candidates with $r_i < f c_{rf}^i / c_{cf}^i$ where r_i is a random number between 0 and 1, f is the ratio between the area of the cluster field and of the reference field, and c_{rf}^i and c_{cf}^i are the completeness of the star (i) in the reference field and the completeness of the closest star in the cluster field, respectively.

The decontaminated CMD is shown in panel (c) of Fig. 4 and confirms that both the eMSTO and the split MS are intrinsic features of the cluster CMD. For completeness, we show the CMD of the subtracted stars in the panel (d) of Fig. 4.

4 THE DOUBLE MS

Having demonstrated that the split MS of NGC 1866 is real, we estimate in the following the fraction of stars in each sequence and the binary fraction. The population ratio as a function of the stellar luminosity and the radial distributions of red MS and blue MS stars are derived in Sections 4.2 and 4.1, respectively.

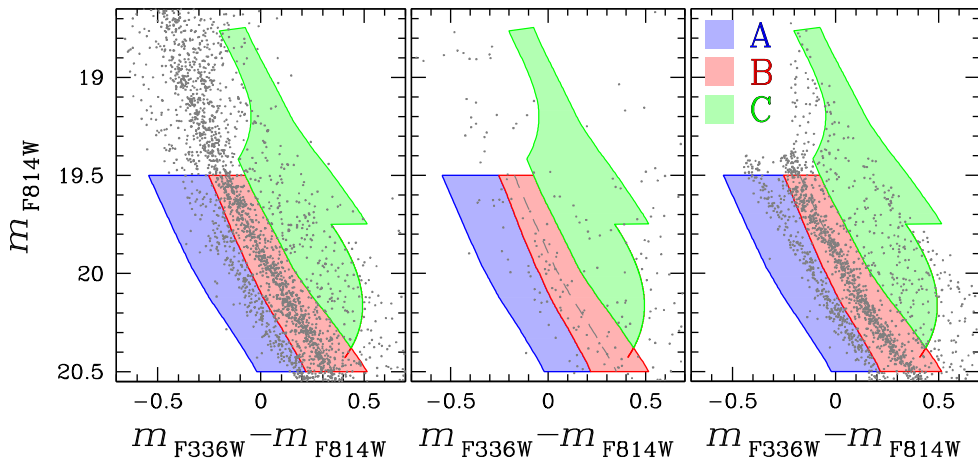


Figure 5. Zoom in of the m_{F814W} versus $m_{F336W} - m_{F814W}$ CMD around the region where the MS split is most prominent. Left-hand and middle panels show the observed CMD for stars in the cluster field and the reference field, respectively. The simulated CMD that best reproduces the observed ones is plotted in the right-hand panel. The shaded areas are the CMD regions A, B, and C used to determine the fraction of red MS and blue MS stars and the binary fraction. See text for details.

In order to infer the fraction of red MS stars, blue MS stars, and the fraction of binaries in the cluster field, we have adapted to NGC 1866 the method described by Milone et al. (2012b, MPB12 hereafter). To do this we have defined three regions in the CMD, namely A, B, and C, which are represented by the blue, red, and green shadow area, respectively, in Fig. 5. These three regions have been derived as follows. Regions A and B are mostly populated by blue MS stars and red MS stars with $19.5 < m_{F814W} < 20.5$, respectively. Note that in the adopted magnitude interval the two MSs are clearly split and binaries with mass ratio $q > 0.5$ are well separated from single MS stars. The blue boundary of region A has been drawn arbitrarily with the criteria of including the majority of blue MS stars. Its red boundary has been determined by shifting each point of the red MS fiducial line by $2\sigma_{\text{colour}}$ towards blue colours, where σ_{colour} is the uncertainty in the $F336W - F814W$ colour determination. The red MS fiducial line has been derived by following the procedure described in section 3.3 of Milone et al. (2016b). Briefly, we have defined a series of $F814W$ magnitude bins of width $\nu = 0.1$ mag in the interval with $18.9 < m_{F814W} < 20.9$. These bins have been determined over a sample of N points separated by steps, $s = \nu/3$, of fixed magnitude (see Silverman 1986 for details). Then we have selected a sample of bona fide red MS stars and calculated the median colour and their mean magnitudes in each magnitude interval. The red MS fiducial has been obtained by interpolating these median colour and mean magnitudes by means of a cubic spline.

The region C defined in Fig. 5 mostly includes binary systems with large mass ratio and has been derived as in MPB12. Its blue boundary is the sequence of binary systems with mass ratio $q = 0.5$ formed by two red MS stars. The red boundary of region C corresponds to the sequence of equal-mass red MS binaries shifted to the red by four times the error in colour. The faint and the bright boundaries correspond to the locus populated by a binary system formed by two red MS stars where the primary component has luminosity $m_{F814W} = 20.5$ and $m_{F814W} = 19.5$. Region B is placed between regions A and C.

We have determined the number of stars, corrected for completeness, in the regions A, B, and C of the cluster-field CMD ($N_{A,B,C}^{\text{CL-F}}$) and of the reference-field CMD ($N_{A,B,C}^{\text{REF-F}}$). We have estimated the number of cluster stars in each region as $N_{A,B,C}^{\text{CL}} = N_{A,B,C}^{\text{CL-F}} - f N_{A,B,C}^{\text{REF-F}}$, where f is the ratio between the area of the cluster field and of the reference field, respectively.

We have generated a large number of CMDs by using ASs and compared them with the observed CMD. Each simulated CMD hosts the same number of region-B stars (N_B^{CL}) as the observed CMD but includes different fractions of blue MS stars, red MS stars, and binaries ($f_{\text{bMS}}, f_{\text{MS}}$, and f_{bin}). Specifically, the grid of simulated CMDs have f_{bMS} and f_{bin} ranging from 0.01 to 1.00 in steps of 0.01. Binaries have been added by assuming a constant mass-ratio distribution in close analogy with what has been observed in Galactic GCs (Milone et al. 2012a, 2016c). Moreover, we have assumed that both the red and the blue MSs have the same binary fraction and that both components of each binary system belong to the same sequence.

To obtain the best match between the simulated and the observed CMDs, we imposed that the simulated CMDs have the same number of stars in the regions A, B, and C as the observed ones. This condition is satisfied when the blue MS hosts 30 ± 2 per cent of the total number of analysed MS stars and for $f_{\text{bin}} = 0.25 \pm 0.02$. For completeness, we have extended the analysis to the entire region with radial distance from the cluster centre smaller than 3.0 arcmin and find slightly higher values for both the fraction of blue MS stars ($f_{\text{bMS}} = 0.35 \pm 0.02$) and the binary fraction ($f_{\text{bin}} = 0.28 \pm 0.02$).

4.1 The population ratio as a function of the stellar luminosity

To investigate the multiple stellar populations along the double MS of NGC 1866, we started to analyse in Fig. 6 the m_{F814W} versus $m_{F336W} - m_{F814W}$ CMD of cluster-field (black points) and reference-field (aqua) stars with $18.9 < m_{F814W} < 20.9$. Only field stars with $r_i < f c_{\text{rf}}^i / c_{\text{cf}}^i$ have been used in the following analysis, in close analogy with what we have done in Section 3.

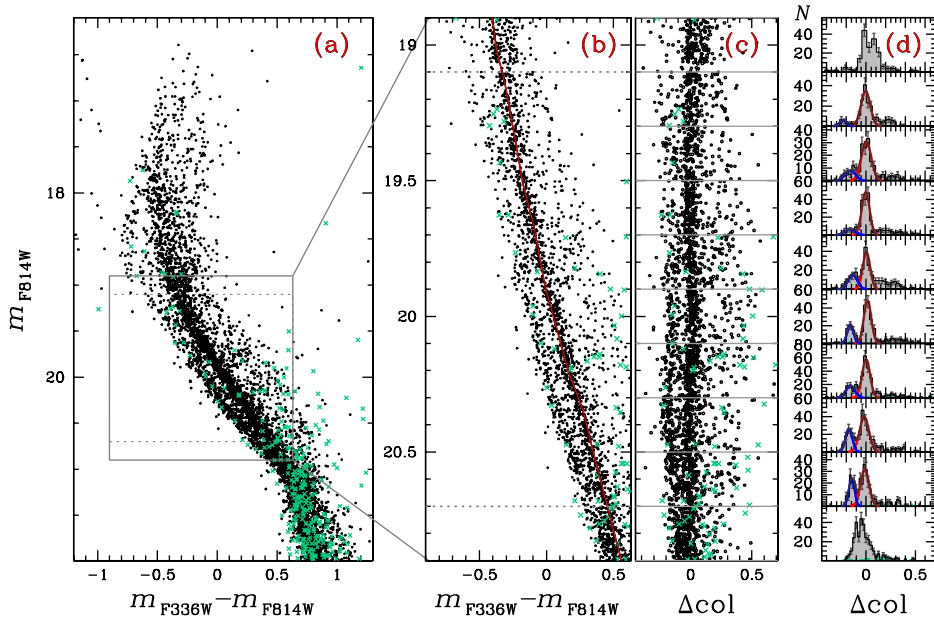


Figure 6. This figure illustrates the procedure used to study the colour distribution of MS stars in NGC 1866. Panel (a) shows the CMD of stars in the cluster field (black points) and in the reference field (green crosses) while panel (b) is a zoom of the analysed MS region. The red line is the fiducial line of the red MS and has been used to derive the verticalized m_{F336W} versus $\Delta(m_{F336W} - m_{F814W})$ CMD plotted in the panel (c). Panel (d) shows the histogram distribution of $\Delta(m_{F336W} - m_{F814W})$ for stars in the 10 $F814W$ magnitude intervals indicated by continuous lines in the panel (c). The histogram distribution of stars with $19.1 < m_{F814W} < 20.7$ is clearly bimodal. The best-fitting least-squares bi-Gaussian function is overimposed to the histograms and the two Gaussian components are coloured blue and red (see text for details).

We plotted in the panel (b) of Fig. 6, a zoom of the CMD for the stars located within the grey box in the CMD shown in the panel (a). The red line is the red MS fiducial derived as in Section 4.

Panel (c) of Fig. 6 shows the verticalized m_{F814W} versus $\Delta(m_{F336W} - m_{F814W})$ CMD. The latter quantity has been obtained by subtracting from the $m_{F336W} - m_{F814W}$ colour of each star the colour of the fiducial at the corresponding $F814W$ magnitude.

The $\Delta(m_{F336W} - m_{F814W})$ histogram distribution of cluster-field stars in 10 mag bins is provided in the panel (d) and confirms the visual impression that the MS is bimodal in the magnitude interval $19.1 < m_{F814W} < 20.7$. We have used a bi-Gaussian function to fit by means of least squares the observed histogram distribution, after the small contribution from reference-field stars has been subtracted. The two Gaussian components that best fit the histograms have been represented with blue and red continuous lines. From the area under the Gaussians, we have inferred the fraction of stars in each interval of magnitude.

The two MS merge together around $m_{F814W} \sim 20.7$ and there is no evidence for a split MS at fainter luminosities. The $\Delta(m_{F336W} - m_{F814W})$ spread significantly increases for $m_{F814W} \lesssim 19.1$, mainly because the analysed sample includes stars in the faintest part of the eMSTO. A small number of blue MS stars is still present in this luminosity interval.

To investigate the properties of the split MS at different luminosities by means of a different method, we have divided the MS region within $19.5 < m_{F814W} < 20.5$ into five intervals of 0.2 mag and we have determined the fraction of blue MS stars and the fraction of binaries with respect to the total number of MS stars in each of them by using the procedure from MPB12 as described in Section 4. In this case we have excluded from the analysis the upper MS, where it is not possible to distinguish binaries with $q > 0.5$ from single MS stars. We have also excluded the faintest MS part due to the poor separation between the blue and the red MSs.

The results are illustrated in the upper panel of Fig. 7, where we plot the fraction of blue MS stars with respect to the total number of MS stars in the cluster field as a function of the $F814W$ magnitude. The grey diamonds indicate the results from the method based on bi-Gaussian fitting while the black dots are obtained from the procedure by MPB12. Red triangles show the derived fraction of binaries as a function of m_{F814W} .

The two methods point to similar conclusions. We find that the blue MS hosts ~ 15 per cent of the total number of MS stars in the brightest analysed magnitude bin and that the fraction of blue MS stars rises up to ~ 33 per cent for $m_{F814W} > 19.7$. We did not find any evidence for a significant variation of the binary fraction with the $F814W$ magnitude in the analysed luminosity interval.

For completeness, we have extended the analysis to the entire region with radial distance smaller than 3.0 arcmin from the cluster centre. The resulting values of f_{bMS} and f_{bin} are shown in the bottom panel of Fig. 7 and confirm the conclusions obtained from the cluster field.

4.2 The radial distribution of the two MSs

In order to investigate how the CMD morphology changes as a function of cluster-centric radius, we have employed two methods in close analogy with what we have done in the study of multiple populations along the MS. The first method is based on bi-Gaussian

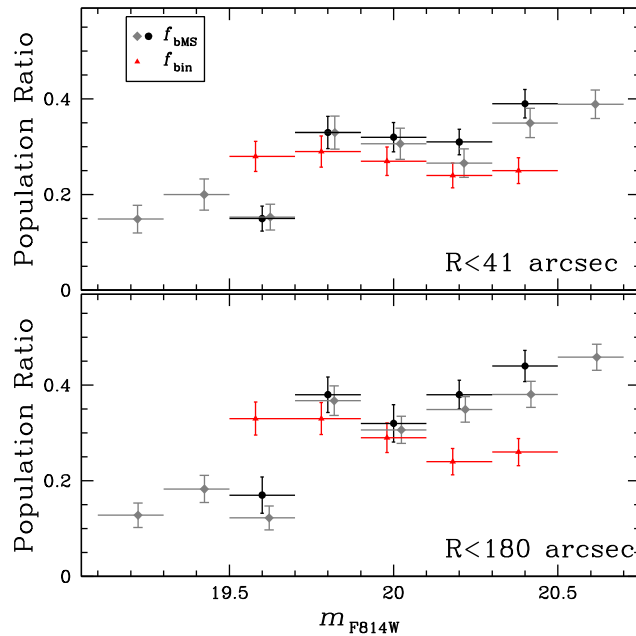


Figure 7. Fraction of blue MS stars (black dots and grey diamonds) and fraction of binaries (red triangles) with respect to the total number of MS stars in different $F814W$ magnitude intervals. Black dots and grey diamonds indicate the results from the MPB12 method and by using the Gaussian-fit method, respectively. The upper panel refers to the cluster field, while the population ratios derived in the region with radial distance smaller than 180 arcsec are plotted in the lower panel. For clarity, the grey and red points have been shifted by ± 0.05 mag with respect to the average magnitude of the stars in the corresponding bin.

fit of the colour distribution of the MS and is illustrated in Fig. 8, where we plot the CMDs of stars in six annuli with different distances from the cluster centre. The inner and the outer radius of each annulus have been chosen in such a way that each CMD includes the same number of stars in the region B. The inset of each panel of Fig. 8 shows the verticalized m_{F814W} versus Δcol diagram for stars in the magnitude interval with $19.5 < m_{F814W} < 20.5$, where the MS split is more evident and where the two MSs run almost parallel.

In the insets of the five CMDs of stars with $R < 3.0$ arcmin, we also plot the corresponding normalized Δcol histogram distribution (grey line). Moreover, we show the histogram of the field stars expected in each annulus (aqua histograms) and the histogram of cluster members (black line) that has been obtained by subtracting the aqua histogram from the grey ones. We have used a bi-Gaussian function to match the black histograms by means of least squares and we have coloured the two components of the best-fitting bi-Gaussians red and blue. All the histograms in each panel have been normalized to the maximum value of the histogram of cluster stars.

The lower-right panel shows reference-field stars with radial distance from the cluster centre larger than 3.0 arcmin. The corresponding histogram of the Δcol distribution is shown in the inset.

Fig. 8 suggests that the fraction of blue MS stars with respect to the total number of MS stars significantly increases when we move from the cluster centre outwards. In particular, from the area under the Gaussians, we find that in the central regions ~ 30 per cent of the total number of MS stars belong to the blue MS, while in the outermost analysed region, the fraction of blue MS stars rises to ~ 45 per cent. The grey diamonds plotted in Fig. 9 show the resulting fraction of blue MS stars (f_{bMS}) as a function of the average radial distance from the cluster centre of all the stars in the bin.

To further investigate the radial distribution of the stellar populations in NGC 1866, we have used the recipe by MPB12 described in Section 4 to determine the fraction of red MS and blue MS stars and the fraction of binaries with respect to the total number of MS stars in each annulus defined above. Results are illustrated in the left-hand panel of Fig. 9 and confirm that the red MS is more centrally concentrated than blue MS stars. As shown in Fig. 9, the binary fraction has a flat distribution for cluster-centric distance smaller than $R \sim 1$ arcmin where their fraction is around 25 per cent. In the cluster outskirts, the binary fraction rises up to $f_{\text{bin}} = 0.38 \pm 0.04$ but this result is significant at the 2σ level only.

Moreover, we have investigated the radial distribution of the stellar populations by using radial bins of fixed size. Specifically, we have chosen 0.25-arcmin radial bins for stars within 1.5 arcmin from the cluster centre and 0.50-arcmin bins for $R \geq 1.5$ arcmin. The large size of the two outermost bins is due to the small number of stars in the external cluster region. Results are illustrated in the right-hand panel of Fig. 9 and confirm the previous finding that red MS stars are more centrally concentrated than blue MS stars. This figure corroborates the idea that the binary fraction increases towards the cluster outskirts and makes it tempting to speculate that a large fraction of binaries are thus associated with the blue MS. A possible exception to these trends is provided by stars in the outermost radial bin with $2.25 < R \leq 3.0$ arcmin but the large error bars prevent us from any firm conclusion.

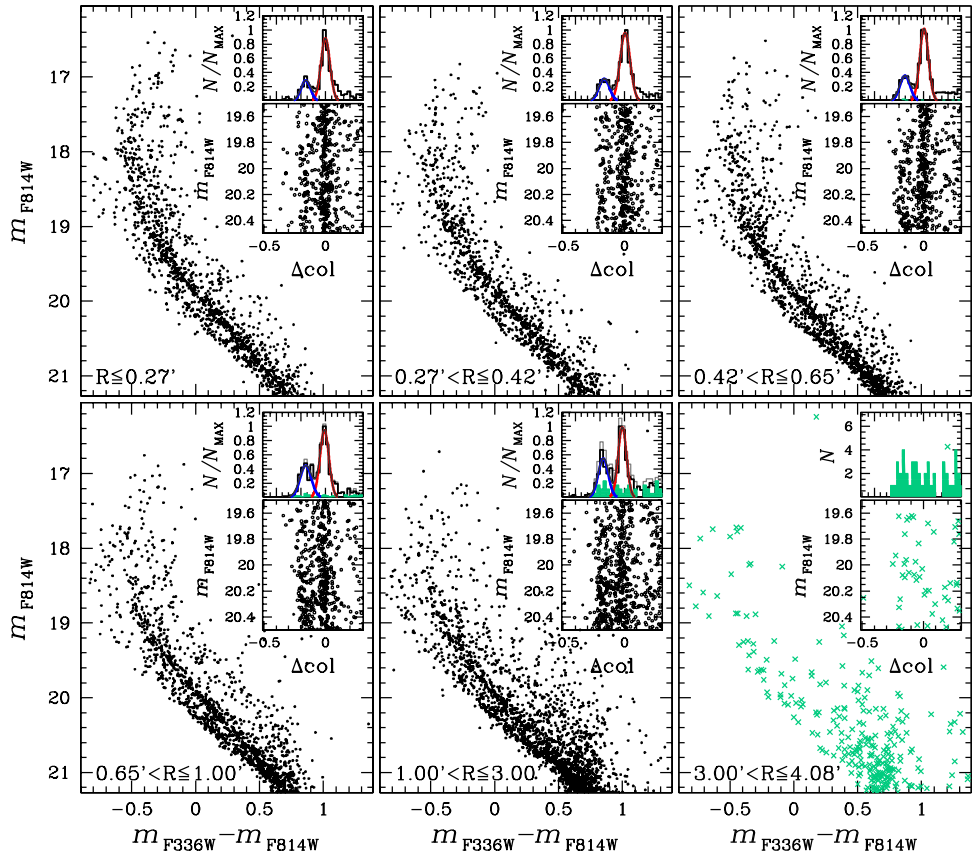


Figure 8. m_{F814W} versus $m_{F336W} - m_{F814W}$ CMDs of stars with different radial distance from the centre of NGC 1866. The verticalized m_{F814W} versus Δcol diagram for stars with $19.5 < m_{F814W} < 20.5$ is plotted in the lower inset of each panel. For the panels of stars within 3 arcmin from the cluster centre, we show the normalized Δcol histogram distribution for all the stars in the inset (grey line), the normalized histogram for field stars (aqua line), and the normalized histogram for cluster members (black line). The shaded aqua histograms correspond to reference-field stars only. The red and blue lines overimposed on the black histogram are the two components of the best-fitting bi-Gaussian function. Reference-field stars are represented with aqua crosses in the bottom-right panel, where we also show the Δcol histogram distribution for all the stars in the inset.

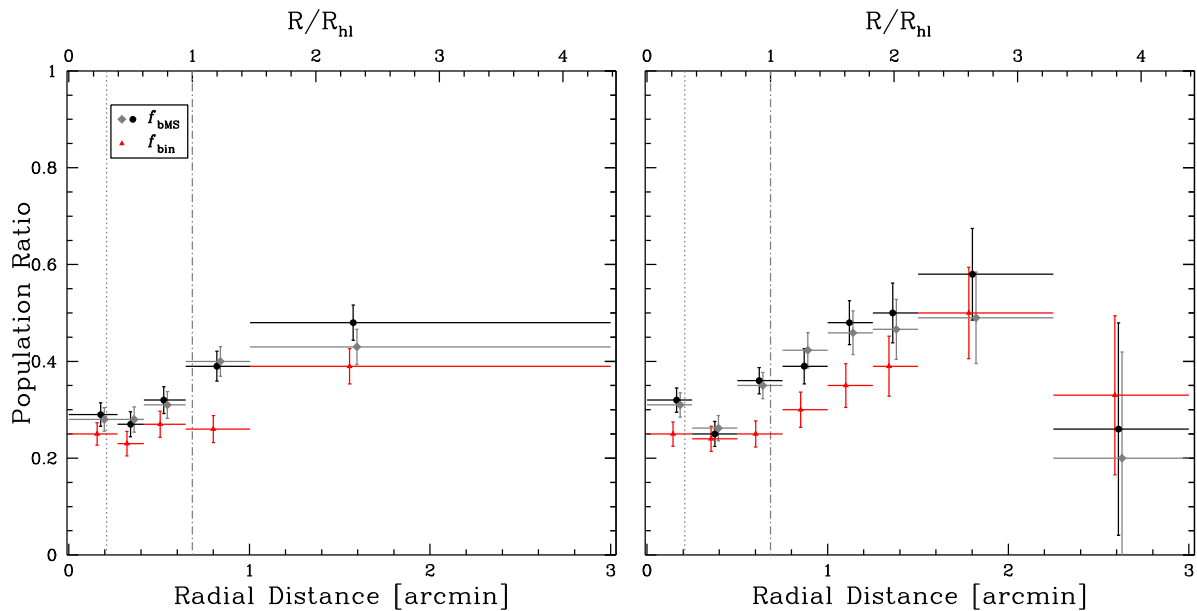


Figure 9. Fraction of blue MS stars with respect to the total number of analysed MS stars as a function of the radial distance from the cluster centre (in arcminutes and in units of projected half-light radius, R_{hl}). The black and grey points with error bars indicate the results obtained from the MPB12 method and the bi-Gaussian-fit method, respectively, as described in the text. Red points show the fraction of binaries in different radial intervals. For clarity, the grey and red points have been shifted by ± 0.03 arcmin with respect to the average radius of stars in each radial bin. The horizontal bars mark the radial extension of each bin. The dotted line and the dashed-dotted vertical line mark the projected core and half-light radius, respectively (McLaughlin & van der Marel 2005). In the left- and right-hand panel plots we have used different radial bins. See text for details.

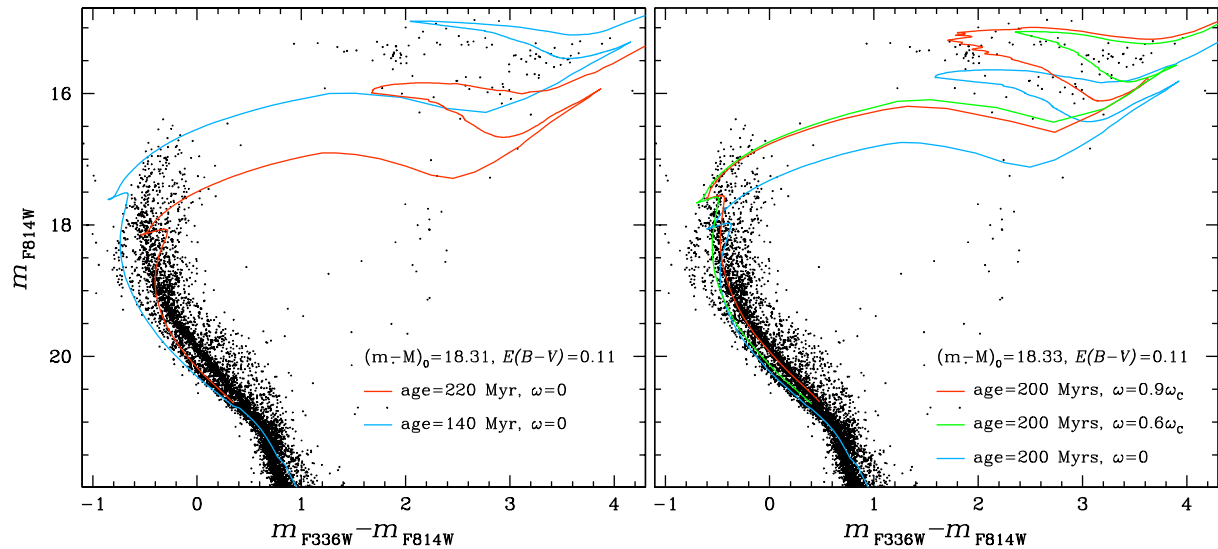


Figure 10. Comparison between the observed CMD of stars in the cluster field and isochrones from the Geneva data base. In the left-hand panel, we have plotted two non-rotating isochrones with different ages while in the right-hand panel, we show three coeval isochrones with no rotation and with rotations of $\omega = 0.6\omega_c$ and $0.9\omega_c$.

5 THEORETICAL INTERPRETATION

The eMSTO and the split MS of young and intermediate-age star clusters have been interpreted both in terms of stellar populations with different rotation rates (e.g. Bastian & De Mink 2009; Niederhofer et al. 2015; D’Antona et al. 2015; Milone et al. 2016a) or with different ages (e.g. Mackey & Broby Nielsen 2007; Milone et al. 2009; Goudfrooij et al. 2014). In addition, Milone et al. (2015) have shown that the eMSTO and the double MS of NGC 1856 are consistent with stellar populations with different metallicity.

In NGC 1866, we can immediately exclude that internal metallicity variations are responsible for the eMSTO and the split MS. Indeed high-resolution spectroscopy of 14 cluster members has revealed neither significant iron spread nor evidence for star-to-star variation of a variety of light elements including sodium, oxygen, and magnesium (Mucciarelli et al. 2011). Similarly, the analysis of eight stars in the eMSTO cluster NGC 1806 shows no evidence for metallicity variations (Mucciarelli et al. 2014; Mackey et al., in preparation). These results demonstrate that the eMSTO and the split MS of NGC 1866, and the eMSTO of NGC 1806 are not due to stellar populations with different Z, and this suggests that similar features observed in the CMDs of other clusters are unlikely due to stars with different metallicity.

In the following subsection, we compare the observed CMD of NGC 1866 with isochrones from the Geneva data base² (Mowlavi et al. 2012; Ekström et al. 2012, 2013; Georgy et al. 2014) that correspond to stellar populations with different ages, while in Section 5.2, we investigate the possibility that the eMSTO and the double MS of NGC 1866 are due to different rotation rates. In the latter subsection, we will also compare the observations with isochrones and synthetic CMDs with both different age and rotation rates.

The comparison between the isochrones and the observed CMD of stars in the cluster field are shown in Fig 10. The adopted values of reddening and distance modulus are quoted in the inset of each panel. The reddening values have been transformed into absorption in the F336W and F814W bands by using the relations between $E(B - V)$, A_{F336W} , and A_{F814W} derived by Milone et al. (2016a).

5.1 Age variation

The comparison between the observed CMD and non-rotating isochrones with the same metallicity but different ages is shown in the left-hand panel of Fig. 10. First we have determined that the blue MS and the brighter eMSTO is well reproduced by a 140-Myr-old population with metallicity $Z = 0.006$, assuming a distance modulus $(m - M)_0 = 18.31$ and reddening $E(B - V) = 0.11$. Then we have searched for an isochrone with the same value of Z that properly fits both the red MS and lower part of the eMSTO. We find that a 220-Myr-old isochrone matches well with the lower eMSTO but provides a very poor fit of the red MS. We conclude that age variation alone cannot be responsible for the eMSTO and the split MS of NGC 1866.

5.2 Rotation

In the right-hand panel of Fig. 10, we investigate the possibility that rotation is the only factor responsible for the double MS and the eMSTO of NGC 1866 by using isochrones with the same age of 200 Myr and different rotation rates of $\omega = 0$ (blue line), $\omega = 0.6\omega_c$ (green line, where ω_c is the critical rotation value), and $\omega = 0.9\omega_c$ (red line). We find that the red MS is well fitted by the fast-rotating stellar population,

² <http://obswww.unige.ch/Recherche/evoldb/index>

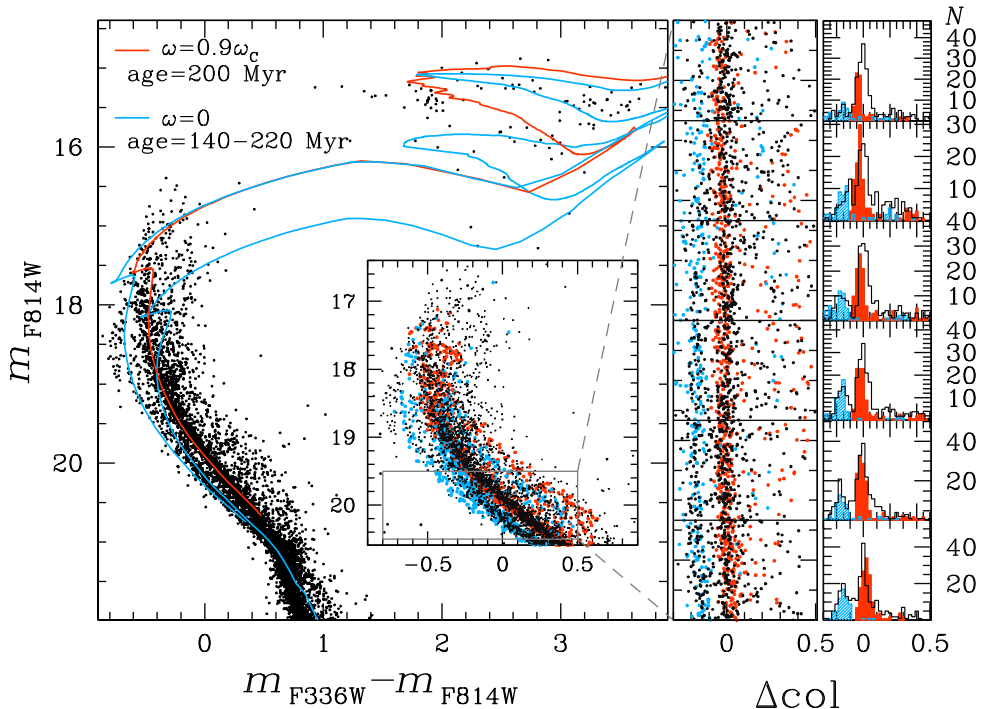


Figure 11. The large panel shows three isochrones from the Geneva data base with different ages and rotation rates, overimposed on the CMD of stars in the cluster field. The red line corresponds to the isochrone with an age of 200 Myr and has a rotational velocity close to the breakout value $\omega = 0.9\omega_c$. The two non-rotating isochrones are coloured cyan and have ages of 140 and 220 Myr. The inset shows a zoom around the upper MS of NGC 1866, where we compare the simulated CMD derived from the rotating (red) and non-rotating (cyan) isochrones and the observed CMD (black). The corresponding verticalized m_{F814W} versus Δcol is plotted in the middle panel, while in the right-hand panels we compare the histogram Δcol distribution of the observed stars in five magnitude intervals and the distribution of the simulated rotating and non-rotating stars. See text for details.

while the blue MS is reproduced by a non-rotating isochrone. Nevertheless, rotation alone does not reproduce the upper part of the blue MS with $m_{F814W} \lesssim 19$.

Finally, we investigate in Fig. 11 the possibility that the observations are consistent with stellar populations with both different ages and different rotation rates. The large panel of this figure shows that a 200 Myr isochrone with rotation $\omega = 0.9\omega_c$ (red line) provides a good fit at the red MS, while the blue MS is well reproduced by two non-rotating isochrones with age of 140 and 220 Myr.

In the inset, we compare the observed CMD of NGC 1866 with a synthetic CMD that includes stellar populations with both age variation and different rotation rates. For that purpose, we have retrieved from the Geneva data base the isochrones plotted in the left-hand panel. Specifically, we have assumed that 70 per cent of total number of the simulated stars have rotation $\omega = 0.9\omega_c$ and the remaining 30 per cent of stars do not rotate. Among them two-thirds have age of 220 Myr and the remaining one-third belong to a younger 140-Myr-old population.

The viewing angle adopted in the simulations follow a random distribution, and the adopted gravity-darkening model from Espinosa Lara & Rieutord (2011) includes the limb-darkening effect (Claret 2000). The synthetic data have been transformed into the observational plane by using the model atmospheres by Castelli & Kurucz (2003) and the transmission curves of the $F336W$ and $F814W$ filters of UVIS/WFC3. The simulated CMD includes a fraction of binaries, $f_{\text{bin}} = 0.25$, which corresponds to the observed value. We have used blue and red colours to represent non-rotating and rotating stars, respectively, while the observed stars are coloured in black.

In the middle panel of Fig. 11, we compare the observed and the simulated verticalized m_{F814W} versus Δcol diagram for MS stars with $19.5 < m_{F814W} < 20.5$. The corresponding Δcol histogram distributions of stars in 5 mag intervals are plotted in the right-hand panels. These figures show that the adopted synthetic models reproduce well the double MS of NGC 1866.

An eMSTO is present in the synthetic CMD, but the fit with the observed CMD is still unsatisfactory. This issue has been previously noticed in both NGC 1856 and NGC 1755 and has been attributed to second-order parameters that affect the hydrogen-burning phase (D'Antona et al. 2015). Indeed the stellar colour and magnitude of stars in the synthetic CMD are strongly affected by the way the convective-core overshoot and the inclination angle are taken into account.

6 SUMMARY AND DISCUSSION

We have used *HST* to derive high-precision photometry of the young LMC cluster NGC 1866 in the $F336W$ and $F814W$ bands of WFC3/UVIS. The resulting CMD reveals that this cluster has a double MS with the blue component hosting about one-third of the total number of MS stars in the analysed magnitude interval. A bimodal MS has been recently observed in other LMC clusters younger than ~ 400 Myr including NGC 1844, NGC 1856, and NGC 1755 (Milone et al. 2013, 2015, 2016a). The finding of a similar feature in NGC 1866 corroborates

the hypothesis that the split MS is a common feature of young MC star clusters. In addition, NGC 1866 exhibits an eMSTO in close analogy with what is observed in most intermediate-age stars clusters of both MCs and in some young LMC clusters (Mackey & Broby Nielsen 2007; Milone et al. 2009, 2015, 2016a; Goudfrooij et al. 2011, 2014; Bastian et al. 2016).

The relative numbers of blue and red MS stars change when moving from the cluster centre to the external regions, with the red MS being more centrally concentrated. While this is the first study on the radial distribution of the multiple MSs in a young cluster, the radial distribution of eMSTO stars in intermediate-age star clusters has been already determined for several clusters by Goudfrooij et al. (2011). These authors find that for several massive clusters the stars in the brightest half of the MSTO region are significantly more centrally concentrated than the stars in the faintest half.

In the cluster field of view, the binary fraction with respect to the total number of MS stars of NGC 1866 is $f_{\text{bin}} = 0.25 \pm 0.02$. The binary fraction is almost constant within ~ 1 arcmin from the cluster centre and seems to increase at larger radial distance, in analogy with what has been observed in the massive young LMC cluster NGC 1805 by Li, de Grijs & Deng (2013).

The comparison between stellar models and the observed CMD rules out the possibility that age variation is only responsible for the split MS of NGC 1866. In contrast, the split MS is well matched by stellar populations with distinct rotation rates. Specifically, the red MS is consistent with an ~ 200 -Myr old population of fast-rotating stars with $\omega = 0.9\omega_c$, while the blue MS is reproduced by non-rotating stars. The adopted stellar models with different age and rotation rates roughly reproduce the eMSTO. As suggested by D'Antona et al. (2015), we speculate that the poor fit is mostly due to second-order parameters adopted in the models that affect the hydrogen-burning phase.

Noticeably, it appears that rotation alone is not able to fully reproduce the observations of NGC 1866. Indeed, while the majority of blue MS stars are possibly coeval, or about 10 per cent older than the red MS, the upper part of the blue MS is reproduced by an ~ 30 per cent younger (~ 140 -Myr-old) stellar population including ~ 15 per cent of the total number of MS stars.

We are aware that the results presented in this work open many more questions than they solve. We regard the preliminary reproduction of the observational features of the CMD, proposed here and shown in Fig. 11, more as a provocative message than as a trustful interpretation. Is it realistic to think that stars born in possibly three different epochs of star formations (~ 140 , ~ 200 , and ~ 220 Myr ago) are present in the cluster? The first consequence of this scenario would be that the first star formation event gives birth to a non-rotating population, the second one to a fast rotating population, and the final burst, ~ 60 Myr later, would include only non-rotating stars. This scheme seems too complex to be realistic, and we should reject it. Nevertheless, the multiple-age scheme may be telling us something on the evolution of these stars.

Also the increase of the blue MS fraction with increasing distance from the cluster centre would argue against the younger age of the blue population. Indeed, if there is an analogy with the multiple populations in old GCs, we expect that second-generation stars are expected to be more centrally concentrated than the first populations (e.g. D'Ercole, D'Antona & Vesperini 2016, and references therein).

Our interpretation of the split MS of NGC 1866 are similar to those by D'Antona et al. (2015) who have shown that the split MS and the eMSTO of the ~ 350 -Myr-old LMC cluster NGC 1856 are consistent with two stellar populations with different rotation rates. In this framework, D'Antona and collaborators attributed the presence of a fraction of non-rotating stars to the braking mechanism of dynamical tides acting on the convective H-burning cores of B-A-type stars due to the presence of a binary companion (Zahn 1977). In fact, observations show that binaries of these spectral types, with periods from 4 to 500 d are synchronized, so they are all slowly rotating (Abt & Boonyarak 2004). If this phenomenon is responsible for the slowly rotating fraction of stars, we could expect that there are more binaries with such adequate periods in the external parts of the cluster.

While it can be straightforward to interpret the populations in the cluster NGC 1856, about a factor of 2 older, by means of two coeval populations, with 70 per cent of fast rotating stars, and ~ 30 per cent of slowly rotating stars, (D'Antona et al. 2015, see above), the case of NGC 1866 looks much more complex. A possible solution is that the stellar populations of NGC 1866 are coeval in close analogy with NGC 1856. As demonstrated in this paper, the recent rotating models (e.g. Ekström et al. 2013; Dotter 2016) make a superb work in reproducing the main features of the observed CMDs. Nevertheless, the way rotation manifests itself in real stars may be not fully captured in the rotating models. If we wish to properly investigate this possibility we must investigate much more deeply the evolution of rotating stars in the braking phase, and examine clusters of different ages to explain the CMDs of these clusters in a coherent scheme. We postpone this analysis to a work in preparation by our group (D'Antona et al., in preparation).

ACKNOWLEDGEMENTS

This paper is based on observations with the NASA/ESA *Hubble Space Telescope*, obtained at the Space Telescope Science Institute, which is operated by AURA, Inc., under NASA contract NAS 5-26555, under GO-14204. We thank the anonymous referee for several suggestions that have improved the quality of this manuscript. APM, AFM, and HJ acknowledge support by the Australian Research Council through Discovery Early Career Researcher Awards DE150101816 and DE160100851 and Discovery project DP150100862.

REFERENCES

- Abt H. A., Boonyarak C., 2004, ApJ, 616, 562
- Anderson J., Bedin L. R., 2010, PASP, 122, 1035
- Anderson J., Bedin L. R., Piotto G., Yadav R. S., Bellini A., 2006, A&A, 454, 1029
- Anderson J. et al., 2008, AJ, 135, 2055
- Bastian N., de Mink S. E., 2009, MNRAS, 398, L11

- Bastian N. et al., 2016, MNRAS, 460, L20
 Bedin L. R., Cassisi S., Castelli F., Piotto G., Anderson J., Salaris M., Momany Y., Pietrinferni A., 2005, MNRAS, 357, 1038
 Bellini A., Anderson J., Bedin L. R., 2011, PASP, 123, 622
 Bertelli G., Nasi E., Girardi L., Chiosi C., Zoccali M., Gallart C., 2003, AJ, 125, 770
 Castelli F., Kurucz R. L., 2003, in Piskunov N., Weiss W. W., Gray D. F., eds, Proc. IAU Symp. 210, Modelling of Stellar Atmospheres. Astron. Soc. Pac., San Francisco, p. A20
 Claret A., 2000, A&A, 363, 1081
 Conroy C., Spergel D. N., 2011, ApJ, 726, 36
 Correnti M., Goudfrooij P., Puzia T. H., de Mink S. E., 2015, MNRAS, 450, 3054
 D'Antona F., Di Criscienzo M., Decressin T., Milone A. P., Vesperini E., Ventura P., 2015, MNRAS, 453, 2637
 D'Ercole A., D'Antona F., Vesperini E., 2016, MNRAS, 461, 4088
 Dotter A., 2016, ApJS, 222, 8
 Ekström S. et al., 2012, A&A, 537, A146
 Ekström A. et al., 2013, Phys. Rev. Lett., 110, 192502
 Espinosa Lara F., Rieutord M., 2011, A&A, 533, A43
 Gallart C. et al., 2003, AJ, 125, 742
 Georgy C., Granada A., Ekström S., Meynet G., Anderson R. I., Wyttenbach A., Eggenberger P., Maeder A., 2014, A&A, 566, A21
 Girardi L., Rubele S., Kerber L., 2009, MNRAS, 394, L74
 Glatt K. et al., 2009, AJ, 138, 1403
 Goudfrooij P., Puzia T. H., Chandar R., Kozhurina-Platais V., 2011, ApJ, 737, 4
 Goudfrooij P. et al., 2014, ApJ, 797, 35
 Gratton R., Sneden C., Carretta E., 2004, ARA&A, 42, 385
 Gratton R. G., Carretta E., Bragaglia A., 2012, ARA&A, 20, 50
 Keller S. C., Mackey A. D., Da Costa G. S., 2011, ApJ, 731, 22
 Li C., de Grijs R., Deng L., 2013, MNRAS, 436, 1497
 Li C., de Grijs R., Deng L., 2014, Nature, 516, 367
 Mackey A. D., Broby Nielsen P., 2007, MNRAS, 379, 151
 Mackey A. D., Broby Nielsen P., Ferguson A. M. N., Richardson J. C., 2008, ApJ, 681, L17
 Marino A. F. et al., 2014, MNRAS, 442, 3044
 Marino A. F. et al., 2015, MNRAS, 450, 815
 McLaughlin D. E., van der Marel R. P., 2005, ApJS, 161, 304
 Milone A. P., Bedin L. R., Piotto G., Anderson J., 2009, A&A, 497, 755
 Milone A. P., Piotto G., Bedin L. R., Cassisi S., Anderson J., Marino A. F., Pietrinferni A., Aparicio A., 2012a, A&A, 537, A77
 Milone A. P. et al., 2012b, A&A, 540, A16 (MPB12)
 Milone A. P., Bedin L. R., Cassisi S., Piotto G., Anderson J., Pietrinferni A., Buonanno R., 2013, A&A, 555, A143
 Milone A. P. et al., 2015, MNRAS, 450, 3750
 Milone A. P. et al., 2016a, MNRAS, 455, 3009
 Milone A. P., Marino A. F., D'Antona F., Bedin L. R., Da Costa G. S., Jerjen H., Mackey A. D., 2016b, MNRAS, 458, 4368
 Milone A. P. et al., 2016c, MNRAS, preprint ([arXiv:1610.00451](https://arxiv.org/abs/1610.00451))
 Mowlavi N., Eggenberger P., Meynet G., Ekström S., Georgy C., Maeder A., Charbonnel C., Eyer L., 2012, A&A, 541, A41
 Mucciarelli A. et al., 2011, MNRAS, 413, 837
 Mucciarelli A., Dalessandro E., Ferraro F. R., Origlia L., Lanzoni B., 2014, ApJ, 793, L6
 Niederhofer F., Georgy C., Bastian N., Ekström S., 2015, MNRAS, 453, 2070
 Piotto G. et al., 2015, AJ, 149, 91
 Renzini A. et al., 2015, MNRAS, 454, 4197
 Silverman B. W., 1986, Monographs on Statistics and Applied Probability. Chapman and Hall, London
 Yang W., Meng X., Bi S., Tian Z., Li T., Liu K., 2011, ApJ, 731, L37
 Yang W., Bi S., Meng X., Liu Z., 2013, ApJ, 776, 112
 Zahn J.-P., 1977, A&A, 57, 383

This paper has been typeset from a TeX/LaTeX file prepared by the author.